Calibration technique for underwater active oneshot scanning system with static pattern projector and multiple cameras

Hiroshi Kawasaki, Hideaki Nakai, Hirohisa Baba
Kagoshima University, Japan
kawasaki@ibe.kagoshima-u.ac.jp

Ryusuke Sagawa
AIST Tsukuba, Japan
ryusuke.sagawa@aist.go.jp

Ryo Furukawa
Hiroshima City University, Japan
ryo-f@hiroshima-cu.ac.jp

Abstract

Underwater 3D shape scanning technique becomes popular because of several rising research topics, such as map making of submarine topography for autonomous underwater vehicle (UAV), shape measurement of live fish, motion capture of swimming human, etc. Structured light systems (SLS) based active 3D scanning systems are widely used in the air and also promising to apply underwater environment. When SLS is used in the air, the stereo correspondences can be efficiently retrieved by epipolar constraint. However, in the underwater environment, the camera and projector are usually set in special housings and refraction occurs at the interfaces between water/glass and glass/air, resulting in invalid conditions for epipolar constraint which severely deteriorates the correspondence search process. In this paper, we propose an efficient technique to calibrate the underwater SLS systems as well as robust 3D shape acquisition technique. In order to avoid the calculation complexity, we approximate the system with central projection model. Although such an approximation produces an inevitable errors in the system, such errors are diminished by a combination of grid based SLS technique and a bundle adjustment algorithm. We tested our method with a real underwater SLS, consisting of custom-made laser pattern projector and underwater housings, showing the validity of our method.

1. Introduction

Underwater 3D shape scanning system becomes important because of various purposes, such as map making of submarine topography, shape measurement of live fish, motion capture of swimming human and 3D sensor for autonomous underwater vehicles (UAV). Structured light systems (SLS) based active 3D scanning systems are widely used for various purposes in the air and are also promising for underwater environments. A typical SLS consists of a camera and a projector where the projector projects an encoded pattern onto an object's surface, images of the object are captured by the camera, and the images are decoded to recover the 3D shape. Because the technique uses an active pattern projector, the correspondence searching process becomes stable by the unique and distinctive patterns, resulting in accurate and dense reconstruction; this makes SLS as popular non-contact 3D shape measurement methods [22, 7]. Among them, one-shot SLS recently attracts many researchers because of its ability to scan dynamic objects [19, 2].

To apply the SLS to the underwater environment, several issues arise. First one is a calibration. For SLS system, usually the intrinsic parameters of the camera and projector as well as the extrinsic parameters are calibrated by using correspondences between a projected pattern from a projector and a captured image by cameras and the shape of the target object. Such correspondence problem can be efficiently solved by epipolar constraint in the air, whereas, the constraint does not hold under the water and the correspondence problem cannot be solved. Another issue is that since common 3D reconstruction techniques are based on central projection model, they cannot be applied to the underwater environment.

In this paper, we propose three approaches to jointly tackle the aforementioned issues. First, we introduce a plane based calibration technique for underwater environment using AR markers [11] on the board to efficiently detect the markers followed by a bundle adjustment to refine the results. Second, to solve the problem of invalid epipolar constraint, we approximate the system with central projection model at specific depth. Since the approximation produces an inevitable errors for searching correspondences, we introduce a grid-based active scanning method, which allows to find correspondences with some tolerance. Finally, we develop a 3D reconstruction algorithm for approximated model, where initial errors are refined by bundle ad-

justment.

In the experiment, we tested and evaluate the effectiveness of the proposed approach using the real system where a projector and cameras are installed in special housings and placed under the water. Currently, the test was conducted at an aquarium pool where water quality is quite good. Even at the aquarium, there are many demands for capturing shapes of live swimming fish, for example, measuring size for health check, acquiring shape deformation to learn swimming mechanisms, etc. We also plan to use the scanner in the sea where water quality is worse.

2. Related Work

Calibration models for underwater camera have been proposed extensively [18, 4, 17, 1, 21, 15, 10, 9, 12]. However, none of them gives an entire calibration and reconstruction procedure for an SLS. Because of the correspondence matching problem in SLS, some of the proposed models becomes invalid since the formulated models do not offer a practical strategy for matching and reconstruction. Besides, projector calibration underwater is also a slightly different issue than camera calibration due to the "blindness" of the projector [5].

There are some early works for underwater 3D reconstruction based on approximation model [18, 4, 17]. Queiroz-Neto *et al*. proposed an underwater model which simply ignores the effects of the refraction, but earns results with low accuracy due to the non-linear refraction effect [18]. Some approximate methods also have been proposed, such as focal length adjustment [18], lens radial distortion approximation [4] and a combination of the two [17]. Unfortunately, the accuracy of these approximation models are also insufficient to an SLS system for correspondence search using epipolar geometry.

To improve the accuracy of underwater measurement, some physical models for camera calibration and reconstruction have been proposed [1, 21, 15, 10, 9, 12]. Agrawal *et al*. gives a general calibration method for underwater cameras, based on a physical refractive model [1]. They consider that all refractive planes are parallel to each other, and they derive front-projection and back-projection equations for their refractive model. However, it is necessary to solve 4th degree equations even for one refractive plane's case, and 12th degree equations in the 2 plane case in a forward projection situation, and thus, it is difficult to use this method directly for SLS. Sedlazeck *et al*. focus on the underwater light rays which are projected as a curved surface: after learning this surface, perspective projection can be done [21]. According to this method, it is also difficult to tackle the forward projection problem due to the complicated learning phase. Kang *et al*. and Sedlazeck also consider the underwater reconstruction with Structure from Motion (SfM) [10, 9]. SfM is a passive way to recover 3D shape of objects, and it is difficult to achieve a dense reconstruction result due to the difficulty of the correspondence searching. Kawahara et.al. proposed pixel-wise varifocal camera model, where the focal length of the projection varies pixel-by-pixel, for modeling non-central projection of an underwater camera, and a calibration method for the cameras [12]. They also proposed an active-stereo system composed of a projector and two cameras, where projection of the cameras and the projector is based on their model [13]. Since image-based correspondence search using epipolar lines are not valid for underwater cameras, they applied space carving method, where only photo-consistency is needed.

In terms of SLS for underwater, Campos *et al*. proposed an underwater active stereo system that uses a DOE-based pattern projector [16]. They used a pattern of parallel lines and each line is not coded into local features. Their decoding method (*i.e*., the method for solving correspondences between the captured image and the projected pattern) relies on the order between the detected lines on the camera image, thus, ambiguity may occur if only a small region of the pattern is detected. Morinaga *et al*. also proposed the active scanning technique using DOE with grid pattern, however, underwater calibration technique is not mentioned [8].

3. Underwater active one-shot scanning system

3.1. System configuration

To use SLS, which consists of a camera and a projector in the underwater environment, the camera and the projector are set into housings, respectively. In addition, we assume that all the cameras are synchronized; note that since the pattern is static, no synchronization is required for a projector. The actual configuration is shown in Fig. 1. We made a waterproof housing as shown in Fig. 2. Left and right housings are for the cameras, while the center housing is for the laser projector with a diffractive optical element (DOE) of a wave pattern; note that energy efficiency of DOE is normally more than 90% and suitable for outdoor environment such as murky water in the sea. One severe problem of DOE is that it can project just a static pattern, and thus, applicable SLS technique is limited; we adopt a grid based technique [20] because of advantages on stability and accuracy. We made our system with two cameras because of the following reasons:

1. It is possible to reconstruct areas which are occluded with one camera, thereby reconstructing a wider area than with conventional monocular camera system.

2. Since projector cannot capture image, bundle adjustment which minimize reprojection error cannot be applied without multiple cameras in real sense.

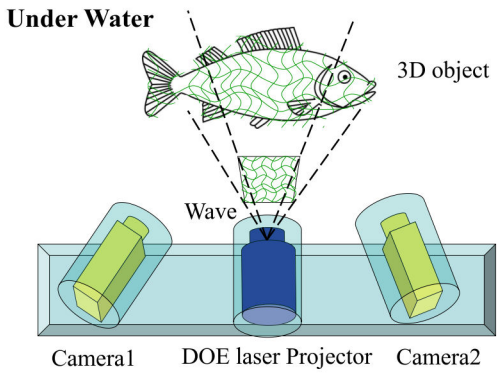

Figure 1. Set up of camera projector camera system in water proof housing.

Figure 2. Real underwater scanning system with two cameras and one DOE laser projector.

3.2. Algorithm overview

Our system consists of mainly two parts, such as calibration part and 3D shape reconstruction part. In the calibration part, we first calibrate the camera intrinsic parameter in the air. Then, we submerge the system into the water and calibrate the system as if it is in the air, *i.e.* we calibrate the system by using central projection model. Since optical mode in the water is not central projection because of refraction, inevitable errors occur and they must be compensated. In our method, they are "undistorted" by polynomial approximation. By applying the polynomial approximation, we have new images with pseudo central projection. Once we get such a central projection images, epipolar constraint holds and correspondences can be efficiently retrieved with some tolerance. Using the correspondences, real intrinsic and extrinsic of the projector parameters as well as parameters for underwater conditions, such as distance and orientation of the interface of air/water, are estimated by bundle adjustment.

In the reconstruction part, we adopt a two-step approach. First, the approximated central projection model is used to perform the wave grid reconstruction to retrieve initial

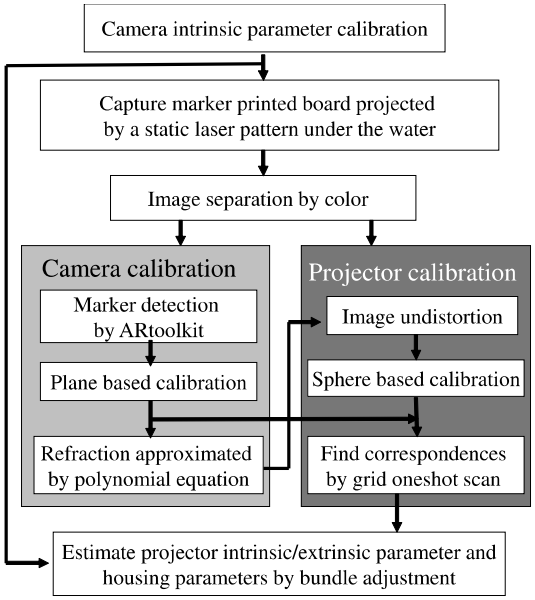

Figure 3. Calibration process in the water.

shape. Then, the estimated 3D points are refined by bundle adjustment using an accurate non-central projection model, which takes into account the refraction. The reason why we need the approximation model for the first step is that a central projection model is not true in the underwater environment, that means epipolar constraint does not hold, however, the epipolar constraint is a key to efficiently find the correspondences with active stereo techniques. Although certain error inevitably occurs with approximation model, they are corrected during the refinement process.

4. Underwater calibration using a planar board

A calibration work-flow is shown in Fig. 3. In the method, first the intrinsic parameters of cameras are estimated by using a planer board in the air [23]. After that, the camera and projector are put into their respective housings and placed under the water. Finally, the intrinsic and the extrinsic parameters of calibration board as well as the housing parameters are estimated.

4.1. Refraction approximated by polynomial equation

Let us consider the full physical refraction model first. We suppose that a camera and a projector are all set into housings respectively, and assume that the housings' thicknesses can be ignored. Based on Snell's law, the following equations are obtained.

$$\frac{\sin\alpha}{\sin\beta} = \frac{\mu_2}{\mu_1} = n, \tag{1}$$

$$\sin\alpha = \frac{x_1}{\sqrt{x_1^2 + y_c^2}}, \sin\beta = \frac{x_b - x_1}{\sqrt{(x_b - x_1)^2 + d^2}}, \quad (2)$$

where coordinate x shows the refractive plane, the refractive indices of the media above and below this plane are μ_1 and μ_2 respectively, b is a 3D point where a ray coming from, $p_1 = (x_1, 0)$ is a point on the interface, d is the distance between the b and camera plane, y_c is the focus of camera, α is the angle of the ray and β is the angle after refraction. After some manipulation, the next equation can be obtained [1],

$$(n^2 - 1)x_1^4 + (-2x_b n + 2x_b)x_1^3 + (x_b^2 n + y_c^2 n - x_b^2 - d^2)x_1^2 - 2x_b y_c^2 n x_1 + x_b^2 y_c^2 n^2 = 0. \quad (3)$$

By solving this 4th order equation, the corresponding epipolar line on the plane of projector pattern with predefined depth can be calculated for each feature points.

In this paper, we propose a polynomial approximation of the full physical refraction model by using the following equation.

$$E(x_1) = \alpha_1 r^2 + \alpha_2 r^4, \quad (4)$$

where r is the distance from the intersection between the optical axis and the interface. Since the equation is same as the lens distortion model, we simply apply openCV library to estimate the parameters; note that the parameter is depth dependent and only valid within a specific depth range.

4.2. Pattern separation and correspondence estimation

Then, a planar board where special markers are printed is projected by the grid pattern projector and captured by the camera. All the captured images are undistorted by the polynomial equation where parameters are estimated in the previous section to be approximated as a central projection model. Those images are separated into two by using color information as shown in Fig. 5 (b) and (c). Then, the intrinsic and extrinsic parameters of cameras are estimated by a planar board calibration technique [23] as if they are in the air. Since the board is projected by a pattern projector, a strong highlight is usually observed interfering a stable detection of checker board pattern. Since the standard algorithm such as openCV [3] requires entire pattern detection for calibration, a highlight is a critical problem. In the paper, we use multiple AR markers [11] instead of checker pattern to realize independent marker detection as shown in Fig. 5 (d). Once markers are detected with several frames, a camera's intrinsic and extrinsic parameters can be estimated efficiently. Note that the estimated parameters are not physically correct, however can be used for further process to find correspondences.

Next, correspondences between a projector pattern and a captured image are estimated. Since a projector cannot capture an image, correspondences should be relatively retrieved by other means. Simple solution is to switching the projected pattern to encode positional information into temporal domain. However, since a static pattern projector is used in our system, such an approach cannot be used and another solution is required. To solve the problem, we take a two step approach, such as a sphere based calibration which requires manual intervention [6] to estimate the initial parameters and a grid-based oneshot scan using the parameters to retrieve dense correspondences. Note that,

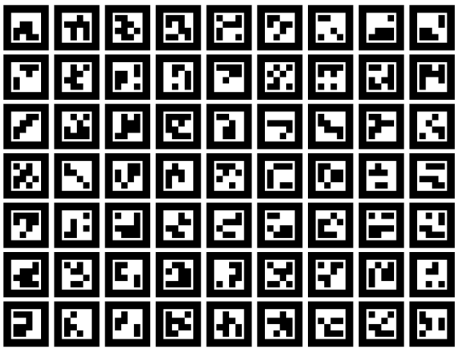

Figure 4. Calibration pattern with AR markers. Minimum Hamming distance is 5.

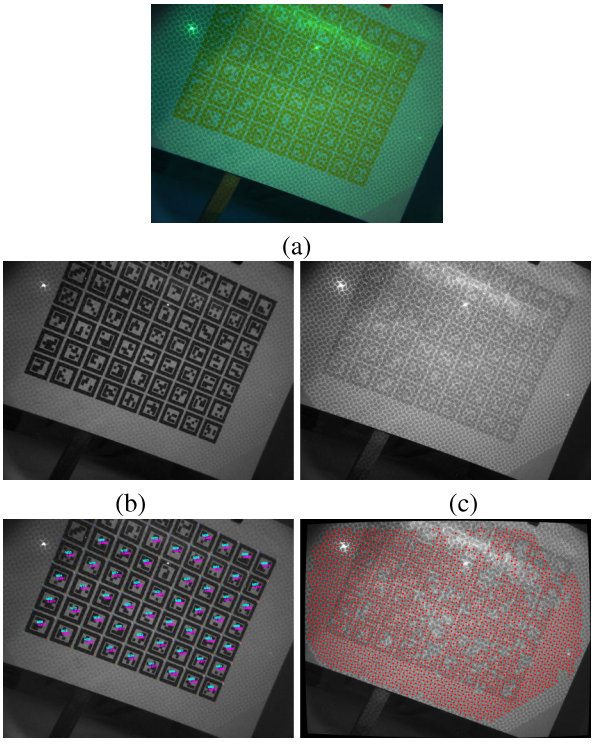

Figure 5. (a) captured image, (b)(c) separated patterns with color information and (d)(e) feature detected results.

since only a single image is required for sphere-based calibration, it is efficient that it makes possible to retrieve dense correspondences from 20-40 frames automatically.

A sphere-based calibration process is as follows. First, images are captured where the sphere is projected by the grid pattern. From the image, points on the spherical contour are sampled manually. Also, the correspondences between the grid points on the camera image and the grid points on the projected pattern are assigned manually. Then, reprojection errors between the captured grid points on the sphere and the simulated grid positions are minimized with respect to the extrinsic parameters, the intrinsic parameters of the projector, and the position of the calibration sphere. Other than the reprojection errors, points on the spherical contour are also used for the optimization. Again, since single image is sufficient for sphere-based calibration, it is not a heavy task.

Once we get the initial parameters by the calibration, we can use epipolar constraint to find correspondences efficiently. Since our system uses wave-grid pattern for projection [20], we can retrieve the correspondences using the same 3D reconstruction algorithm and results are shown in Fig. 5(e) red points. We can confirm that dense correspondences are estimated.

4.3. Projector intrinsic/extrinsic and housing parameters estimation

In the previous step, the intrinsic and extrinsic parameters for each camera and projector is estimated, however, they are based on approximated central projection model. To estimate the real parameters, we conduct bundle adjustment using the retrieved correspondences. For evaluating errors for bundle adjustment, the back projected 3D points from projector in camera coordinate system are reprojected to camera planes by using the intrinsic parameter of projector A, extrinsic parameters between projector and the kth camera $\theta_k = (R_k, t_k)$, extrinsic parameters θ_i for planar board at frame i, and housing parameters $\phi_k = (\vec{n}_k, d_k)$ as shown in Fig. 6. The sum of squares of each distance between each projected point and corresponding detected point on the camera plane is calculated by the following equation:

$$\underset{A,\theta_i,\theta_k,\phi_k,\phi_p}{argmin} \sum_{i,j,k} Reproj(\theta_k, \phi_k, Proj(\theta_i, \phi_p, p_{ij})) - c_{ijk}, \tag{5}$$

where p_{ij} is the jth point on the ith frame of projector pattern, c_{ijk} is the corresponding points on the captured image of the kth camera, $Proj(\theta_i, \phi_p, x)$ is a function to calculate 3D position on the board i, and $Reproj(\theta_k, \phi_k, X)$ is the 4th oder equation (3) to calculate the reprojection on a camera plane considering refraction. In the paper, we use the Levenberg-Marquardt algorithm for optimization.

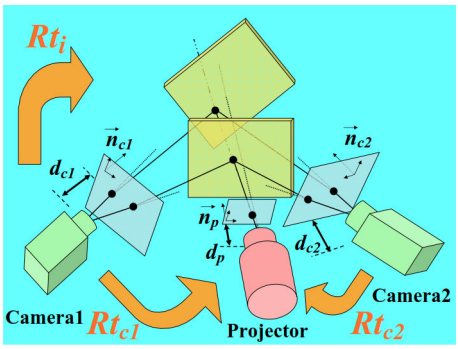

Figure 6. Positions of glasses (d and $\vec{n}$) are estimated through calibration process in the water.

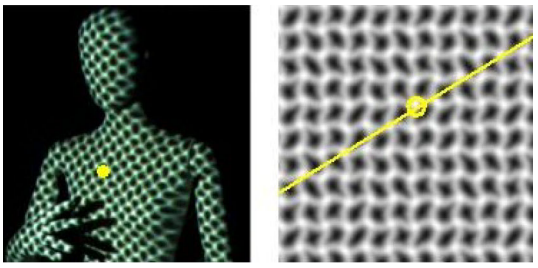

(a) (b)

Figure 7. (a) Corresponding point and (b) Epipolar line for (a).

5. Oneshot 3D reconstruction under the water

5.1. Wave grid reconstruction

For 3D reconstruction, it is necessary to find matches between points on the image plane and the known projector pattern. In our method, we use a "wave pattern" because of the distinctiveness and uniqueness of its features and its reconstruction density [20]. Fig. 7 is an example of the pattern. The correspondences are found through an epipolar search. During the search, the impact of our polynomial approximation on accuracy is limited since the interval between intersections in the wave grid is much larger than the pixel width, and an error of a few pixels does not affect the correspondence search. This feature is important for our underwater scanning method because the polynomial approximation inevitably will create some errors on the epipolar lines. Since the reconstructed results have some errors because of approximation model and inconsistent shapes because of depth dependent calibration parameters, those errors are effectively solved in the refinement process.

5.2. Refinement with bundle adjustment

Refinement of 3D shape will be conducted by the following way. We set 3D points to be estimated with bundle adjustment. Since we can retrieve a hundred of corresponding points between camera and projector image through the

wave reconstruction process, we can calculate the reprojection error by simply solving the fourth order polynomial equation (3).

Since we can start the optimization from the initial shape calculated by the approximated model, it converges quickly with Leaven-Marquardt algorithm with our implementation. It should be noted that, since the images are undistorted by the parameter of approximation model in the underwater environment to retrieve the initial shape, the image is needed again distorted by the approximation parameters and undistorted by ordinary distortion parameters which are estimated by openCV in the air before the bundle adjustment.

6. Experiments

6.1. Real system calibration

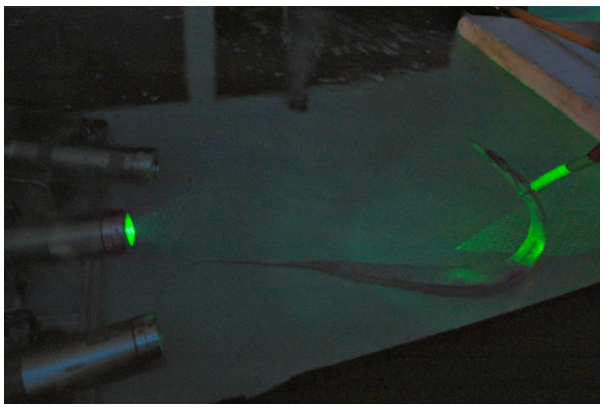

Figure 8. Experimental environment of underwater scan.

First, we conducted the underwater calibration process with the real environment as shown in Fig. 8. Camera we use is Grasshopper with resolution 1600*1200, and special pattern projector using diffractive optical element (DOE). AR marker printed planar board for calibration is set at the distance near 0.8m from the camera and the projector, and for each orientation, we just adjust the angle of the planar board but keep the position of it. Before submerging the system into the tank, we take 50 pictures of the planar board for calibrating the camera-projector system in air, and estimate the intrinsic and extrinsic parameters of the camera and projector [14]. After that, the system was put injected into the tank. We took 50 pictures for calibrating the system underwater as shown in Fig. 9(a) and (b) and estimate the extrinsic parameters, the polynomial approximation parameters and position of the housing glass at this time. The final calibration result after optimization is 0.74 of re-projection error for camera, and 0.53 pix for projector as shown in Fig. 10 where we can confirm that the reprojection error is drastically decreased after optimization. We

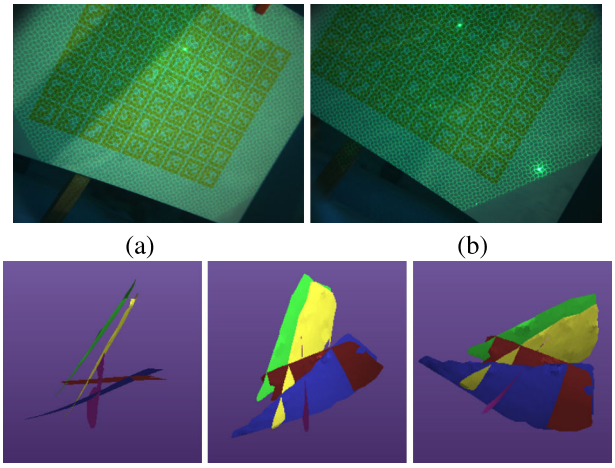

Figure 9. (a) and (b) captured scenes of planar board with AR marker and (c)-(e) reconstructed shapes after estimation of the extrinsic parameters of each board with bundle adjustment algorithm.

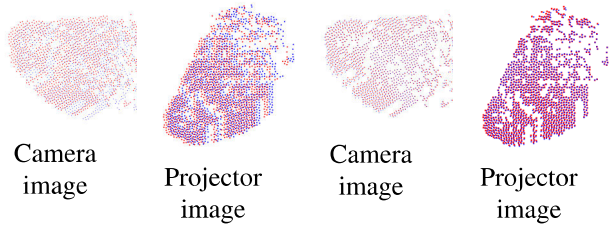

Figure 10. Reprojection of camera and projector image. Blue: observed points and Red: reprojected points.

can also confirm That the estimated planer board is almost flat in Fig. 9(c-e) verifying our calibration process.

6.2. Shape refinement by bundle algorithm

Then, we captured and reconstructed the 3D shape of a sphere and swimming fish using wave reconstruction. Fig. 11(a)(b)(g) and (h) shows the example of captured image and Fig. 11(c)(d)(i) and (j) shows a reconstruction results. Since two cameras are used for our system and both cameras are calibrated independently, reconstructed shapes for each camera do not coincide as we can see in the results. Such gap can be eliminated and integrated with our refinement algorithm. As shown in Fig. 11(e)(f)(k) and (l), we can confirm that the our refinement algorithm successfully integrate two shapes into single consistent shape. For quantitative evaluation, we calculate RMSE for the planar board by fitting the plane to the board and it was drastically decreased from 9.7mm to 0.7mm, confirming the effectiveness of our algorithm.

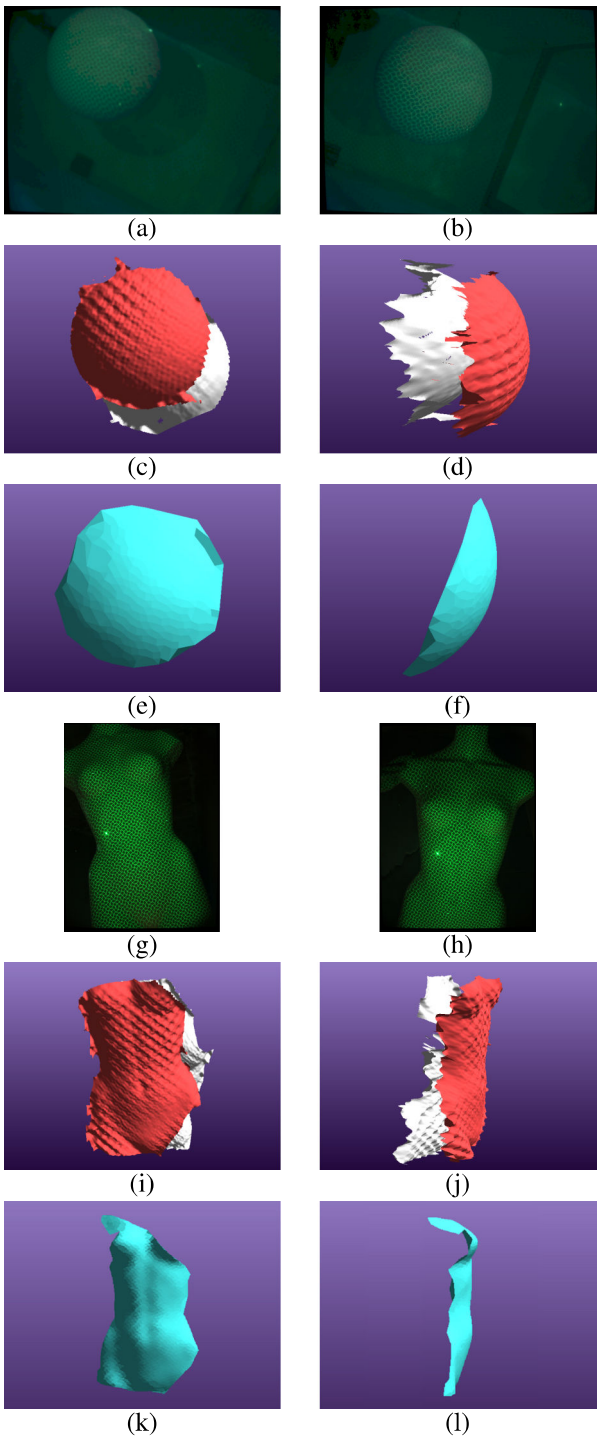

Figure 11. Captured images and reconstruction results of the sphere and the mannequin. (a)(b)(g)(h) Captured images by left and right camera. (c)(d)(i)(j) White shapes are reconstructed by left camera and red shapes are reconstructed by right camera. (e)(f)(k)(l) Light blue shapes are integrated shapes with bundle adjust algorithm.

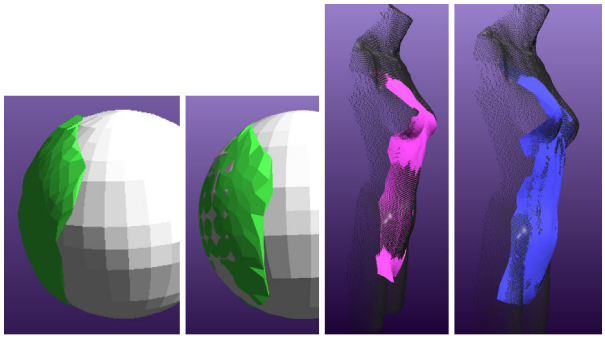

Figure 12. Reconstructed shapes with/without bundle adjustment. The left figures are before bundle adjustment and the right figures are after bundle adjustment. We can clearly see that shapes are getting closer to the ground truth with a bundle adjustment.

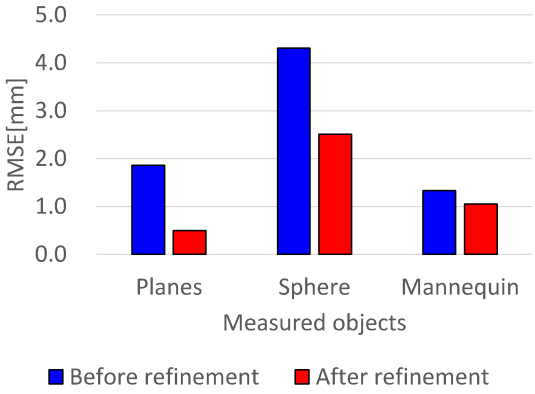

Figure 13. Shape accuracies before and after refinement process of section 5.2.

6.3. Evaluation of 3D shape improvements by refinement

Next, we evaluated accuracies of the 3D shapes before and after the refinement process of section 5.2. We measured three types of shapes, which are a set of planes, a ball, and a mannequin. Distances from the camera and the objects are around $500mm$ for all the cases. Their shapes are reconstructed as shown in Fig. 12. Then, the shape accuracies of intermediate and final results are evaluated. For the set of planes, the reconstructed points are fitted to planes by PCA, and the residual RMSEs are calculated. For the sphere and the mannequin shape, the ground-truth shape data are fitted to the reconstructed point sets using ICP algorithm, and the residual RMSEs of the ICP is used for evaluation. The ground-truth shape of the sphere is synthetically generated, whereas the ground-truth shape of the mannequin is captured in advance using gray code projection in the air. The results are shown in Fig. 13. From the results, the shape RMSEs of the final results are shown to be small (less than $0.5mm$ for the bast case, and about $2.5mm$ for the worst case). For all the cases, the residual errors from the ground-truth shapes are improved by the refinement process.

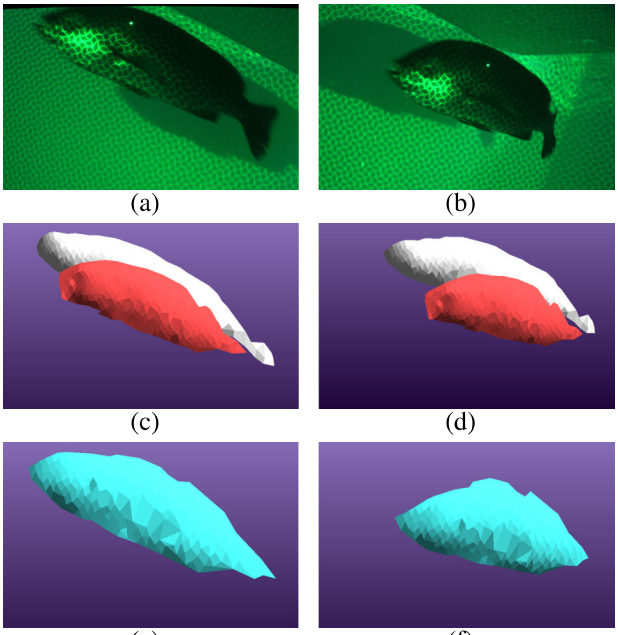

Figure 14. Captured images and reconstruction results of the live swimming fish. (a)(b) Captured images by left and right camera. (c)(d) White shapes are reconstructed by left camera and red shapes are reconstructed by right camera. (e)(f) Light blue shapes are integrated shapes with bundle adjust algorithm.

6.4. Example results of scanning fish

Finally, we captured live fishes in the pool at aquarium. Since our technique requires just a single shot for reconstruction, non-rigid and moving shapes can be reconstructed. We believe that there is no other systems which can reconstruct a swimming fish in underwater environment. Fig. 14 show the captured images from the left and right cameras and their reconstruction results. Fig. 15 show the results of swimming fish. Left column shows a sequence of captured images and right column shows reconstructed shapes. From the results, we can confirm that the swimming fish is successfully reconstructed.

7. Conclusion and Future Work

In this paper, we propose a practical calibration technique to apply oneshot active 3D scanning method in the underwater environment. To realize the system, we propose three solutions. First, we calibrate the camera and projector parameters with polynomial approximation as well as planar board based calibration technique. Then, shapes are reconstructed by wave reconstruction which allows inevitable errors in epipolar geometry. Finally, 3D shapes are refined by the bundle adjustment algorithm which calculates the actual 2D position on the image plane by solving the fourth order polynomial of physical model. Experiments are conducted with real environment showing the effectiveness of our method. Robust reconstruction technique under water environment is our future work.

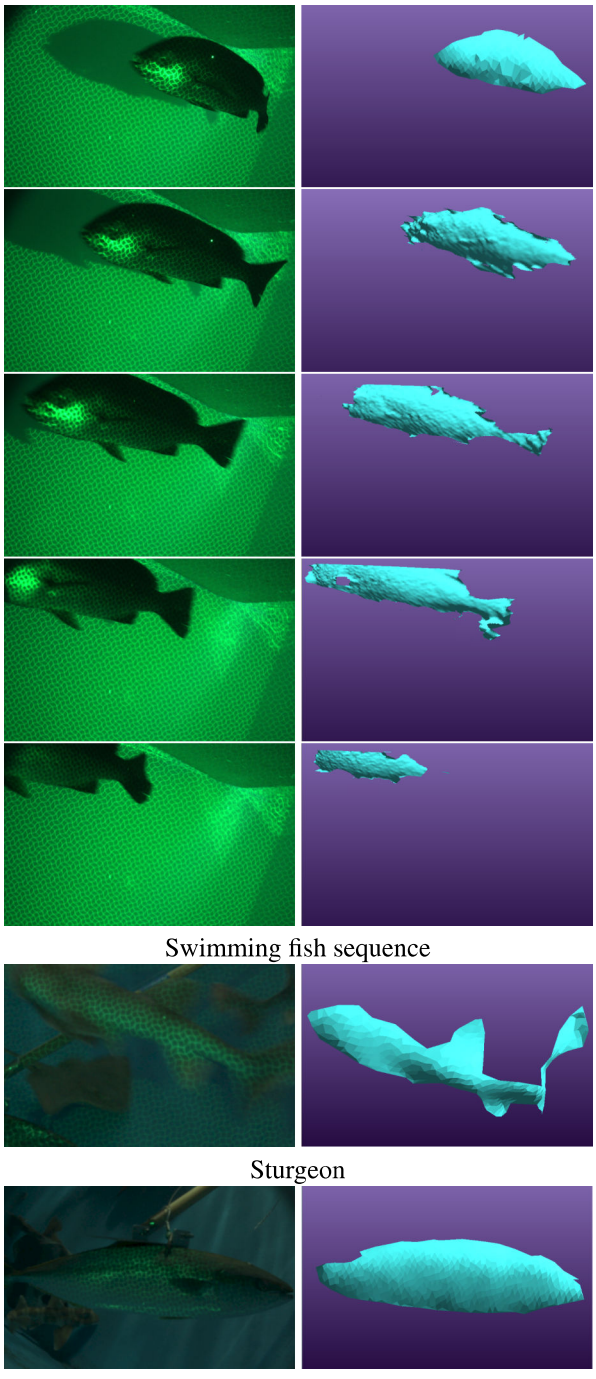

Figure 15. Captured scene (left column) and reconstructed 3D shapes (right column).

Acknowledgment

This work was supported in part by MSR CORE12.

References

[1] A. Agrawal, S. Ramalingam, Y. Taguchi, and V. Chari. A theory of multi-layer flat refractive geometry. In *CVPR*, 2012.

[2] H. Aoki, R. Furukawa, M. Aoyama, S. Hiura, N. Asada, R. Sagawa, H. Kawasaki, T. Shiga, and A. Suzuki. Noncontact measurement of cardiac beat by using active stereo with waved-grid pattern projection. In *Engineering in Medicine and Biology Society (EMBC), 2013 35th Annual International Conference of the IEEE*, pages 1756–1759. IEEE, 2013.

[3] G. Bradski. The OpenCV Library. *Dr. Dobb's Journal of Software Tools*, 2000.

[4] R. Ferreira, J. P. Costeira, and J. A. Santos. Stereo reconstruction of a submerged scene. In *Pattern Recognition and Image Analysis*, pages 102–109. Springer, 2005.

[5] X. Fu, Z. Wang, H. Kawasaki, R. Sagawa, and R. Furukawa. Calibration of the projector with fixed pattern and large distortion lens in a structured light system. In *The 13th IAPR Conference on Machine Vision Applications*, 2013.

[6] R. Furukawa, M. Aoyama, S. Hiura, H. Aoki, Y. Kominami, Y. Sanomura, S. Yoshida, S. Tanaka, R. Sagawa, and H. Kawasaki. Calibration of a 3d endoscopic system based on active stereo method for shape measurement of biological tissues and specimen. In *EMBC*, pages 4991–4994, 2014.

[7] O. Hall-Holt and S. Rusinkiewicz. Stripe boundary codes for real-time structured-light range scanning of moving objects. In *ICCV*, volume 2, pages 359–366, 2001.

[8] M. Hiroki, B. Hirohisa, V.-S. Marco, K. Hiroshi, F. Ryo, and S. Ryusuke. Underwater active oneshot scan with static wave pattern and bundle adjustment. In *Image and Video Technology: 7th Pacific-Rim Symposium, PSIVT 2015*, pages 404–418, Auckland, New Zealand, 2015. Springer International Publishing.

[9] A. Jordt-Sedlazeck and R. Koch. Refractive structure-from-motion on underwater images. In *Computer Vision (ICCV), 2013 IEEE International Conference on*, pages 57–64. IEEE, 2013.

[10] L. Kang, L. Wu, and Y.-H. Yang. Two-view underwater structure and motion for cameras under flat refractive interfaces. In *Computer Vision–ECCV 2012*, pages 303–316. Springer, 2012.

[11] H. Kato and M. Billinghurst. Marker tracking and hmd calibration for a video-based augmented reality conferencing system. In *Proceedings of the 2nd International Workshop on Augmented Reality (IWAR 99)*, San Francisco, USA, Oct. 1999.

[12] R. Kawahara, S. Nobuhara, and T. Matsuyama. A pixel-wise varifocal camera model for efficient forward projection and linear extrinsic calibration of underwater cameras with flat housings. In *Computer Vision Workshops (ICCVW), 2013 IEEE International Conference on*, pages 819–824. IEEE, 2013.

[13] R. Kawahara, S. Nobuhara, and T. Matsuyama. Underwater 3d surface capture using multi-view projectors and cameras with flat housings. *IPSJ Transactions on Computer Vision and Applications*, 6(0):43–47, 2014.

[14] S. Kiyota, H. Kawasaki, R. Furukawa, and R. Sagawa. Efficient projector calibration method using plane with checkerboard pattern. In *Information Processing Society of Japan (IPSJ) Technical Report*, volume 2012-CVIM-180, pages 1–8, 2012.

[15] J.-M. Lavest, G. Rives, and J.-T. Lapresté. Underwater camera calibration. In *ECCV*, pages 654–668. Springer, 2000.

[16] M. Massot-Campos and G. Oliver-Codina. Underwater laser-based structured light system for one-shot 3d reconstruction. In *SENSORS, 2014 IEEE*, pages 1138–1141. IEEE, 2014.

[17] O. Pizarro, R. Eustice, and H. Singh. Relative pose estimation for instrumented, calibrated imaging platforms. In *DICTA*, pages 601–612. Citeseer, 2003.

[18] J. P. Queiroz-Neto, R. Carceroni, W. Barros, and M. Campos. Underwater stereo. In *Computer Graphics and Image Processing, 2004. Proceedings. 17th Brazilian Symposium on*, pages 170–177. IEEE, 2004.

[19] R. Sagawa, Y. Ota, Y. Yagi, R. Furukawa, N. Asada, and H. Kawasaki. Dense 3D reconstruction method using a single pattern for fast moving object. In *ICCV*, 2009.

[20] R. Sagawa, K. Sakashita, N. Kasuya, H. Kawasaki, R. Furukawa, and Y. Yagi. Grid-based active stereo with single-colored wave pattern for dense one-shot 3D scan. In *3DIMPVT*, pages 363–370, 2012.

[21] A. Sedlazeck and R. Koch. Calibration of housing parameters for underwater stereo-camera rigs. In *BMVC*, 2011.

[22] M. Young, E. Beeson, J. Davis, S. Rusinkiewicz, and R. Ramamoorthi. Viewpoint-coded structured light. In *CVPR*, June 2007.

[23] Z. Zhang. A flexible new technique for camera calibration. *Technical Report MSR-TR-98-71*, 12 1998.